Journal of Materials Chemistry

Cite this: J. Mater. Chem., 2011, 21, 5114

www.rsc.org/materials

PAPER

Improved performance of flexible dye-sensitized solar cells by introducing an interfacial layer on Ti substrates

Chia-Hua Lee,[ac] Wei-Hao Chiu,[b] Kun-Mu Lee,[a] Wen-Feng Hsieh[b] and Jenn-Ming Wu*[c]

Received 26th November 2010, Accepted 24th January 2011
DOI: 10.1039/c0jm04099a

The recombination reaction of injected electrons with triiodide ion in the electrolyte limits the efficiency of dye-sensitized solar cells (DSSCs). This study reports the preparation of a sponge-like and conformal TiO_2 underlayer by hydrogen peroxide oxidation of Ti foil. This underlayer serves as a charge recombination barrier layer at the nanocrystalline TiO_2/substrate interface, and suppresses the recombination reaction. This sponge-like TiO_2 underlayer increases the electrical contact area between the Ti substrate and nanocrystalline TiO_2, helping nanocrystalline TiO_2 attach to the Ti substrate. This study compares the performance of DSSCs that were subjected to different Ti surface treatments. Electrochemical impedance spectroscopy results confirm that the proposed sponge-like TiO_2 underlayer increased the open-current voltage (V_{OC}) and fill factor (FF) due to prolonged electron life time (τ_{eff}), and minimized resistance at the TiO_2/Ti interface (R_{CT}). With an optimal thickness of nanocrystalline TiO_2 and concentration of I_2, we achieved a conversion efficiency of 6.75% for a back-illuminated DSSC.

Introduction

Dye-sensitized solar cells (DSSCs) are promising low cost solar cells with high conversion efficiencies. Solar cell made of TiO_2 nanoparticles film fabricated on heavy, rigid and expensive fluorine-doped tin-oxide (FTO) glass substrates offer the best efficiency of 11%.[1] Lightweight and flexible substrates, such as plastic or metal foil, enable roll-to-roll mass production and make it possible to extend DSSCs to new applications. However, the thermal instability of plastic substrates limits the TiO_2 sintering temperature to approximately 150 °C. This low temperature leads to poor necking of TiO_2 nanoparticles, and decreases the performances of solar cell devices.[2] Therefore, researchers have proposed using metal substrates, such as Ti, W and stainless steel, to obtain a flexible DSSC with high-temperature sintered TiO_2.[3–7] A high-temperature sintering process can improve the interconnection between TiO_2 particles and substrates adhesion, achieving high conversion efficiency. Ti metal foils are an excellent alternative to plastic substrates due to their low sheet resistance, good flexibility, superior corrosion resistance, and high-temperature tolerance.[6]

To improve cell performance, previous researchers have introduced thin charge recombination layers into the conducting substrate/TiO_2 interface to decrease the charge recombination loss.[8–12] The spray pyrolysis deposition of a thin TiO_2 blocking layer on FTO can control the dark current.[8] The atomic layer deposition of a conformal TiO_2 underlayer may also passivate surface states.[9] A TiO_2-WO_3 composite layer coated between FTO and TiO_2 improves electrical contact at the interface.[10] The effects of a blocking layer on photovoltaic performance may vary because blocking layers can affect the optical, electrochemical, or adhesion properties of transparent conductive oxide (TCO) substrate DSSCs.[11] Therefore, the role of an underlayer is difficult to define. The underlayers on the TCO have increased the open-circuit voltage (V_{OC}),[8,9] short-circuit current density (J_{SC}) or both.[10,12] Frank *et al.* reported that recombination occurs predominantly at the substrate instead of the entire TiO_2 film. Although the role of the underlayer remains debatable, suppressing the recombination at the conducting substrate/TiO_2 interface helps obtain high-efficiency DSSCs.[13]

Most underlayer research focuses on TCO substrate DSSCs, with only a few reports on metallic substrates. Preparing both SiO_x and ITO layers on a stainless steel substrate enhances the efficiency by suppressing the dark current.[14] Yun *et al.* reported that roughening the substrates increased the performance of a stainless substrate DSSC due to enhanced electrical contact at the TiO_2/metallic substrate interface.[5] The preparation of an underlayer on the Ti substrate typically involves the dip-coating method.[3,15] To improve the performance of Ti substrate DSSCs, it would be worthwhile to investigate the effects of Ti substrate surface treatment.

This study investigates the effects of physical and chemical treatments on Ti foil surface properties and photovoltaic

[a]*Green Energy & Environment Research Laboratories, Industrial Technology Research Institute, Hsinchu, 310, Taiwan. E-mail: wu408410@yahoo.com.tw; Fax: +886-3-5722366; Tel: +886-3-5162227*
[b]*Department of Photonics & Institute of Electro-Optical Engineering, National Chiao Tung University, Hsinchu, 300, Taiwan*
[c]*Department of Materials Science and Engineering, National Tsing-Hua University, Hsinchu, 300, Taiwan*

performances of DSSCs. Results show that the oxidation of metallic Ti by hydrogen peroxide (H_2O_2), and thereby the formation of an amorphous TiO_2 underlayer on the Ti substrate, is an efficient way to modify the Ti substrate. Electrochemical impedance spectroscopy (EIS) confirms that this underlayer enhanced DSSC performance. This study explores the optimal conditions for back-illuminated DSSCs and investigates the effects of thickness of TiO_2 and concentration of I_2 on photovoltaic properties.

Experimental

Ti substrate surface treatment

Commercial Ti foil substrates (0.25 mm thickness, 99.9% purity, Fuu Cherng Co. Ltd., Taiwan) were used as photoanode substrates (sample 1-as-received). The Ti substrate surface was polished and smoothed using an abrasive (sample 2-polished). The resulting thin layer of metal oxide tarnish was removed after the polishing process. Chemical treatment was then performed by soaking the Ti foils in 0.04 M $TiCl_4$ aqueous solution at 70 °C for 30 mins (sample 3-$TiCl_4$ and sample 4- polished/$TiCl_4$). Direct oxidation treatment was performed by soaking each Ti foil (5×10 cm^2) in 50 mL of 30 wt % hydrogen peroxide solution at room temperature for 48 h (sample 5-H_2O_2). The Ti foil substrates were then cleaned with a detergent solution, and rinsed with DI water, acetone, and ethanol.

DSSCs fabrication

Anatase TiO_2 particles were synthesized using the sol–gel method.[16] The nanocrystalline TiO_2 was dispersed in α-terpineol (Fluka) with ethyl cellulose as binder to form a TiO_2 paste.[16] Photoelectrode films were prepared on Ti foil substrates using the screen printing method. The photoelectrodes were heated at 500 °C for 1 h under an air atmosphere. The area of the active electrode was 0.283 cm^2. The photoelectrodes were immersed in a solution of 0.5 mM *cis*-bis(isothiocyanato)bis-(2,2′-bipyridyl-4,4′-dicarboxylato)-ruthenium(II) bis-tetrabutylammonium (Solaronix, N719) in a mixed solvent of 1 : 1 acetonitrile and *tert*-butanol at room temperature for 24 h. The dye-loaded photoelectrodes were then rinsed with acetonitrile to remove the remaining dye. The counter electrode was made by dropping a H_2PtCl_6 (Showa) isopropanol solution on FTO glass (2.2 mm thickness, 8–10 Ω/sq, Pilkington TEC glass) and heating it at 400 °C for 20 min. The dye-loaded photoelectrodes were separated by 60-μm-thick hot-melt spacers (Dupont, Surlyn) with counter electrodes. The internal space of the cell was filled with an electrolyte solution containing iodine redox couple consisting of 1,1-methyl-3-propylimidazolium iodide (PmII, Merk), I_2 (Sigma-Aldrich), LiI, and *tert*-butylpyridine (TBP, Sigma-Aldrich) in acetonitrile.

Measurements

The morphologies of the Ti foil surface with physical and chemical treatments, including as-received, $TiCl_4$ treated, polished, polished and $TiCl_4$ treated, and H_2O_2 treated, were observed by a field emission scanning electron microscope (FESEM) (JEOL, JSM-7000F) operated at 10 KeV. The Raman spectra were carried out using an Ar ion laser operating at 514.5 nm on a Jobin-Yvon T64000 microspectrometer with a 1800 grooves/mm grating in a backscattering configuration. The film thicknesses of photoelectrodes were measured by a Microfigure Measuring Surfcorder (Kosaka Laboratory, ET3000). The overall energy conversion efficiency was evaluated using a xenon lamp (Yamashita Denso, YSS-100A) with a light intensity of 100 mW cm^{-2} (AM1.5). The incident light intensity was calibrated with a standard silicon photodiode (Bunko Keiki, BS-520). The evolution of the electron transport process in the cell was investigated using electrochemical impedance spectroscopy (EIS). Impedance spectroscopy was performed using an electrochemical analyzer (Autolab, PGSTAT30). Impedance measurements were carried out by applying a DC bias at open circuit voltage (V_{OC}) and an AC voltage with an amplitude of 10 mV in a frequency range from 10^{-2} Hz to 10^5 Hz under AM1.5G illumination.

Results and discussion

Characterization of Ti surface treatments

Fig. 1 shows the morphology and the structure of the Ti foil surface with and without surface treatments. Fig. 1(a) and 1(b) shows the surface morphologies of the as-received and polished Ti substrates, respectively. After $TiCl_4$ chemical treatment, the surface morphology of the Ti substrates did not change obviously (not shown here). When H_2O_2 oxidized the surface of the Ti foil substrate, it created the porous and conformal titania, shown in Fig. 1(c) and 1(d). The cross-sectional SEM image in

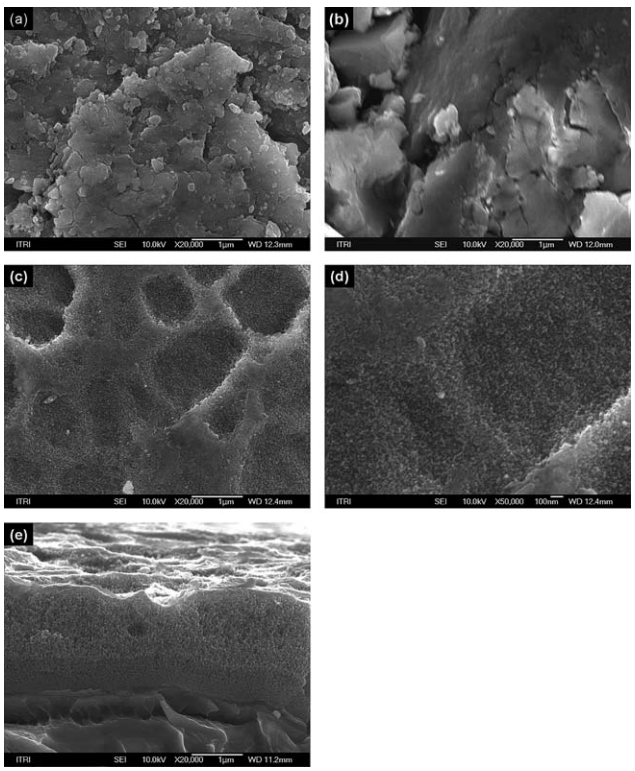

Fig. 1 SEM images of Ti substrates (a) as-received, (b) polished, (c, d) H_2O_2 treated. (e) is cross-sectional images of H_2O_2 treated substrate.

Fig. 1(e) shows that the H_2O_2-oxidized Ti foil had a porous TiO_2 layer, approximately 1 μm thick, forming a TiO_2 layer with a sponge-like structure.

Fig. 2 (a) and 2 (b) show the Raman spectra of as-received, polished, and H_2O_2 treated Ti foils and these Ti foils after annealing, respectively. The as-received Ti foil exhibited a Raman shift at 149 cm^{-1} and 644 cm^{-1} which are attributed to anatase TiO_2. No specific Raman shift appeared on the Ti foil surfaces modified by polishing process and H_2O_2 oxidization. This indicates that the Ti foil surface after polishing or H_2O_2 treatment exhibits no TiO_2 crystalline structure (Fig. 2a). On the other hand, the Ti foils exhibited considerable difference after annealing, as shown in Fig. 2 (b). After annealing, the as-received Ti foil exhibited Raman shifts at 149 cm^{-1} and 644 cm^{-1} (anatase structure) and 235 cm^{-1}, 449 cm^{-1} and 610 cm^{-1} (rutile structure). The as-received Ti foil showed an improvement in intensity after annealing, implying an increase in film crystallinity. The polished and H_2O_2 oxidized Ti foils exhibited Raman shifts at 449 cm^{-1} and 610 cm^{-1}, and the lack of a strong band in the 140–150 cm^{-1} region suggests that the surface of polished and H_2O_2 oxidized Ti foils transformed into a crystalline rutile TiO_2 underlayer. After annealing, the change in crystallinity of the interfacial layer would lead to the change of charge transfer resistance at the Ti/TiO_2 interface, as discussed later.

The effects of Ti surface treatment on DSSC Performance

Table 1 summarizes the photovoltaic characteristics of DSSCs constructed by different surface treatments of the Ti photoelectrode substrates under AM 1.5G illumination. The J_{SC} is in a range of 9.35–10.10 mA cm^{-2} for Ti foil with or without $TiCl_4$ treatment, polished, and polished/$TiCl_4$ treatment. This suggests that the polished and $TiCl_4$ treatments have no obvious influence on J_{SC}. The V_{OC} fluctuates between 0.69 and 0.71 V for the as-received and polished devices, but it improves slightly for devices with $TiCl_4$ treatment compared to the polished-only samples. The filling factor (FF) of devices using as-received and $TiCl_4$ treated Ti foils was exceptionally lower than the others. Polishing treatment increased the FF from 0.36 and 0.37 to 0.73 and 0.76 for DSSCs without $TiCl_4$ and with $TiCl_4$ treatment, respectively. This indicates that the removal of the passive tarnish oxide layer on the Ti foil substrate decreased the electrical contact resistance between the Ti foil/nanocrystalline interface. In contrast, H_2O_2 oxidized Ti foil exhibited a significant improvement in the V_{OC} and FF of the DSSC. Although the H_2O_2 treated Ti foil formed a porous TiO_2 underlayer which could contribute to J_{SC}, the best efficiency was achieved by a dramatically improvement in V_{OC} and FF.

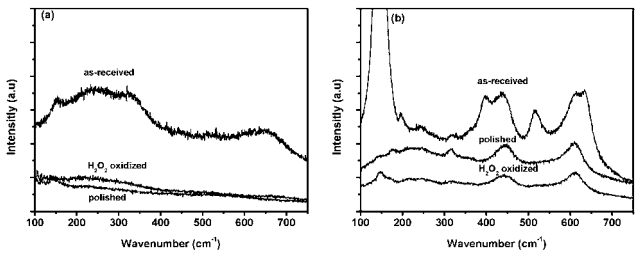

Fig. 2 Raman spectra of the as-received, polished and H_2O_2 treated Ti substrates (a) without annealing and (b) after annealing.

Table 1 Photovoltaic performances, series resistance (R_S) and charge transfer resistance (R_{CT}) of DSSCs used Ti foil as photoelectrode substrates with different surface treatments. The thicknesses of photoelectrodes are 20 μm

Surface treatment	J_{SC}/mAcm^{-2}	V_{OC}/V	FF	η (%)	R_S/Ω	R_{CT}/Ω
None	9.35	0.70	0.36	2.35	4.25	47.7
$TiCl_4$	10.10	0.70	0.37	2.58	5.38	47.1
Polished	10.01	0.69	0.73	5.11	5.87	1.48
Polished/$TiCl_4$	9.70	0.71	0.76	5.24	5.22	1.36
H_2O_2	10.91	0.73	0.77	6.20	5.79	1.29

This study uses electrochemical impedance spectroscopy (EIS) to characterize the electron transporting properties involved in these complex photovoltaic devices to clarify the effects of Ti foil surface treatments on DSSC performance. A diffusion-recombination model based equivalent circuit was used to extract the electron transport parameters in the DSSCs,[17,18] as Fig. 3(a) shows. The circuit elements relating to photoelectrodes include the electron transport resistance ($R_w = r_wL$)in the TiO_2 network, the charge transfer resistance ($R_k = r_k/L$), which relates to recombination of electrons at the TiO_2/electrolyte interface, and the chemical capacitance ($C_\mu = c_\mu L$) of the TiO_2 photoelectrode. Some circuit elements are used to modify the equivalent circuit model.[19] These elements include the series resistance (R_S) of the conductive substrates (Ti foil and FTO) and external circuits, the impedance of the diffusion of I_3^- in the electrolyte (Z_N), the charge-transfer resistance (R_{Pt}) and the interfacial capacitance (C_{Pt}) at the Pt/electrolyte interface, the charge-transfer resistance (R_{Ti}) and the interfacial capacitance (C_{Ti}) at the uncovered Ti foil/electrolyte interface, and the resistance (R_{CT}) and the capacitance (C_{CT}) at the Ti foil/TiO_2 interface. Impedance spectra of cells using as-received, $TiCl_4$ treated, polished, polished/$TiCl_4$ and H_2O_2 treated Ti substrates are shown in Fig. 3 (b) and 3 (c). The first high frequency semicircle corresponds to the charge transfer behavior at the Pt/electrolyte (R_{Pt} and C_{Pt}), the uncovered Ti/electrolyte (R_{Ti} and C_{Ti}) and the Ti/TiO_2 (R_{CT} and C_{CT}) interfaces. The second semicircle at intermediate frequency is mainly resulted from the nanocrystalline TiO_2 film, including R_w, R_k and C_μ. The low frequency arc of impedance component is contributed from diffusion of I_3^- in electrolyte (Z_N).[17–19]

Table 1 lists the series resistance (R_S) and the resistance at the Ti foil/TiO_2 interface as estimated from the Nyquist plots in Fig. 3 (b). The series resistance (R_S) is the sum of the resistance of two conductive substrates and the resistance of external circuits. Table 1 shows that the R_S of the DSSC made of the as-received Ti foil was 4.25 Ω, while those with different surface treatments increased to 5.22–5.79 Ω. Assuming that the resistance of external circuits and FTO of counter electrodes remained unchanged, these changes in the R_S value may be due to the surface treatment of the Ti foil. These results suggest that all surface treatment processes cause a slight increase in the ohmic contact resistance of the Ti foil and external circuits. However, surface treatments had an obvious influence on the resistance at the Ti foil/TiO_2 interface (R_{CT}). The R_{CT} of devices with as-received or $TiCl_4$ treated Ti foils is 47.7 and 47.1 Ω,

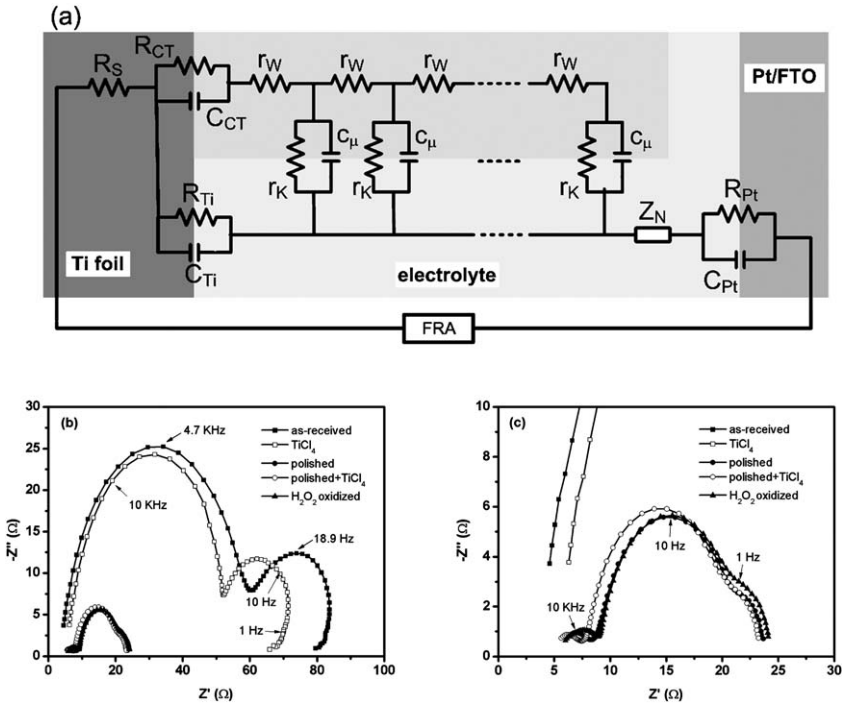

Fig. 3 (a) Equivalent circuit for the simulation of the impedance spectra of the DSSCs. (b, c) Nyquist plots of DSSCs with different surface modification on the Ti substrates. The enlarged spectra of (b) are shown in (c).

respectively, while those of the polished only and polished/$TiCl_4$ treated Ti foils significantly decrease to 1.48 and 1.36 Ω, respectively. Only a slight difference in R_{CT} appeared after forming an underlayer fabricated by $TiCl_4$ on as-received and polished Ti foils, indicating that the interfacial resistance at the TiO_2/Ti foil was reduced slightly. However, the polishing process remarkably decreases the R_{CT} of DSSCs. This observed decrease in R_{CT} could be attributed to the removal of the passive tarnish layer created on the renewed Ti surface. This renewed surface could transform into an amorphous TiO_2 thin layer that could be favorable for attaching to nanocrystalline TiO_2 during the annealing process. These results agree with that of Yanagida *et al.*, who found that the deposited Ti by sputtering transformed into a TiO_x thin layer after annealing and improved the electrical contact at the TiO_2/substrate interface.[20] The slight change of R_S in this study shows that the R_{CT} plays a major role in the FF of DSSCs composed of the Ti foils. Compared with the DSSCs constructed by polished Ti, the amorphous TiO_2 underlayer prepared by H_2O_2 oxidation achieved the lowest R_{CT}. The formation of a thin TiO_2 underlayer improved adhesion, and thus decreased the R_{CT}. Another possible explanation is that the porous TiO_2 underlayer increases the electrical contact area between the nanocrystalline TiO_2 and Ti foils of the devices. This result supports previous research on DSSC of stainless steel substrate that also shows a decrease in R_{CT} by increasing the surface area of the substrates.[5] These findings suggest that the sponge-like structure and amorphous phase of the TiO_2 underlayer played a role in promoting the FF of DSSCs. EIS results confirm that the porous TiO_2 underlayer prepared by H_2O_2 oxidation has decreased the R_{CT} value, thereby minimizing the total resistance of the cell and improving FF.

To investigate the influences of polishing and H_2O_2 oxidation on photovoltaic performances, the parameters were further extracted from Fig. 3(c) to analyze the electron transport behavior. Table 2 lists the steady-state electron density in the TiO_2 conduction band (n_S), the ratio of R_w/R_k, the effective lifetime of electrons (τ_{eff}), the mean electron transit time (τ_d), and the charge collection efficiency (η_{cc}). The V_{OC} of DSSCs are the differences between the Fermi level of TiO_2 and the redox potential of I^-/I_3^-. A higher electron density (n_S) leads to negative shift in the Fermi level of the TiO_2 photoanode of the H_2O_2 treated device, which could be the main reason for the V_{OC} of this DSSCs being larger than that of polished or polished/$TiCl_4$ devices. The observed increase in n_S can be attributed to suppressing the recombination reactions at Ti/TiO_2 interfaces by introducing a favorable and connective underlayer on the Ti substrate. The reciprocal of the characteristic frequency ($1/\omega_{max}$) represents the mean electron lifetime (τ_{eff}) of the TiO_2 photoanode. The underlayer formed by $TiCl_4$ deposition prolonged the τ_{eff} and the underlayer prepared by H_2O_2 oxidation of Ti foil had the highest τ_{eff}. This indicates that the underlyer limited the recombination reaction, which is consistent with the improvement in V_{OC}. The injected electrons undergo forward transport in the TiO_2 film and recombination with I_3^- ions. The mean electron transit time, τ_d, can be calculated according to $\tau_d/\tau_{eff} = R_w/R_k$. As Table 2 shows, H_2O_2 treated Ti substrates had the lowest τ_d, Again, this reveals that the porous TiO_2 underlayer formed by H_2O_2 oxidized Ti foil can enhance the electron transport in the TiO_2 photoanode. To estimate the charge collection capability of DSSCs, the charge collection efficiency (η_{CC}) can be estimated according to the relation of $\eta_{cc} = 1-\tau_d/\tau_{eff}$.[21] The η_{CC} improved from 60.4% to 71.1% and 73.0% for the polished/$TiCl_4$ and H_2O_2 treated devices, respectively. These

Table 2 The electron transport properties of DSSCs constructed by Ti foil with physical/chemical surface treatments evaluated by EIS

Ti foil surface treatment	n_S/cm^{-3}, 10^{18}	R_w/R_k	τ_{eff}/ms	τ_d/ms	η_{CC} (%)	L_{eff}/μm
Polished	2.75	0.340	79.3	31.3	60.4	25.4
Polished/$TiCl_4$	3.24	0.290	97.9	28.3	71.1	29.7
H_2O_2	3.63	0.270	102.7	27.7	73.0	30.8

results indicate that the formation of the TiO_2 underlayer by H_2O_2 successfully prevented the recombination with I_3^-. Based on EIS observations, the porous TiO_2 underlayer formed by H_2O_2 oxidized Ti foil improved the electrical contact at the Ti substrate and the electron transport in nanocrystalline TiO_2 film, increasing both FF and V_{OC}.

Effect of TiO_2 thickness on photovoltaic performance

In previous research,[22] the performance of front-illuminated DSSC is largely dependent on TiO_2 film thickness. A part of the incident light transmitted through the electrolyte is absorbed by the electrolyte in the case of back-illuminated DSSCs. There, it is worthy to investigate the effect of film thickness on performance in back-illuminated DSSCs. Fig. 4 shows the effect of film thickness on J_{SC}, FF, V_{OC}, and η of DSSCs using H_2O_2 treated Ti substrates. The film thickness of TiO_2 had a significant influence on J_{SC}. The J_{SC} initially increased with TiO_2 film thickness from 12 to 28 μm but saturated with a further increase in film thickness. Unlike the tendency of J_{SC}, the V_{OC} slightly decreased as the film thickness of photoanode increased. This decrease in the V_{OC} is generally due to the higher charge recombination, with more limited mass transport in the thicker photoanodes. The fill factor did not exhibit an obvious declining trend. The FF is known to be determined by the total series resistance of the cell, including the resistances of the Ti substrate, the photoanode, the electrolyte, and the counter electrode. This non-declining trend of FF could be attributed to the decrease in R_{CT} at the Ti/TiO_2 interface without significantly increasing the resistance of the TiO_2 photoanode as the TiO_2 film thickens. The changes of FF and V_{OC} corresponding to changes in the thickness of the photoelectrode are less significant than the change of J_{SC}. Therefore, the thickness dependence of the overall conversion efficiency is primarily due to J_{SC}. The optimal thickness of the photoelectrode was approximately 28 μm for the back-illuminated DSSCs in this study.

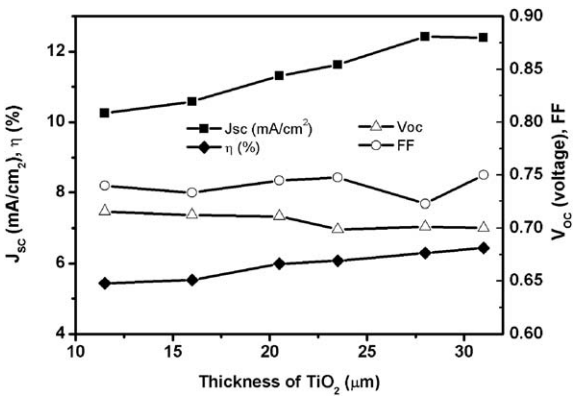

Fig. 4 The effect of TiO_2 photoelectrode thickness on photovoltaic characteristics of N719-sensitized solar cells: short-circuit current density (J_{SC}), open-circuit voltage (V_{OC}), fill factor (FF), and overall energy conversion efficiency (η).

Concentration effect of I_2 in electrolyte

The space between the photoande and the counter electrode is filled with the electrolyte, which normally contains the I^-/I_3^- redox couple that partially absorbs incident visible light. Thus, the concentration of I_3^- should affect DSSC performance. For front-illuminated based devices, a sufficient concentration of the I^-/I_3^- redox couple is needed for cell operation. The J_{SC} usually increases with an increase in the concentration of I_2. The I^-/I_3^- redox couple resulted in more extent of absorbing visible light in the back-illuminated devices than in front-illuminated based ones. Therefore, it is important to study the influence of the concentration of I_2 on performance of back-illuminated DSSC. Table 3 summarizes the influence of the concentration of I_2 on various parameters of the H_2O_2 treated Ti foil-based DSSCs obtained with the optimized TiO_2 photoelectrode thickness of 28 μm. The J_{SC} of the DSSCs depended strongly on the concentration of I_2;a high concentration of I_2 led to an increase in FF, whereas both J_{SC} and V_{OC} exhibited declining trends with increasing I_2.

Fig. 5(a) shows the impedance spectra of cells with various I_2 concentrations. Table 3 shows that the electron lifetime τ_{eff} decreases as the concentration of I_2 increases. An increase in I_2 concentration should increase concentration of I_3^-, which in turn increases the recombination rate. The decrease in τ_{eff} indicates that the recombination of electron increased, which is consistent with the decrease in V_{OC} in devices with a higher I_2 concentration. The decreasing trend in V_{OC} and τ_{eff} was attributed to increasing recombination reaction.

The low frequency arc of impedance component was reported depending on diffusion of I_3^- in electrolyte. Table 3 summarizes the peak frequency of the low frequency arc (ω_{max}) and DC resistance of diffusion of I_3^- (R_D). According to the equation $D_1 = (1/2.5)\delta^2\omega_{max}$, the decrease of I_3^- concentration does not affect the diffusion coefficient of I_3^- (D_1). In this equation, δ represents the thickness of liquid electrolyte. This suggests that the concentration of I_3^- is the major influence on R_D instead of the diffusion behavior of I_3-.[23] The reduction of I_3^- concentration increased R_D, which is accompanied with an increase in the total resistance, as Fig. 5 (a) shows. The reduction of I_3^- concentration caused increased R_D, enlarged total resistance, and low FF value.

J_{SC} is generally determined by the light harvesting efficiency, charge injection yield of dye molecules, and charge transport of a device. Using the same dye as sensitizer, the charge injection yield of devices with various concentrations of I_2 should be

Table 3 Photovoltaic performances, electron life time (τ_{eff}), effective electron diffusion length (L_n) and dc resistance of impedance of diffusion of I_3^- (R_D) evaluated by EIS

Electrolyte I_2/M	J_{SC}/mA cm^{-2}	V_{OC}/V	FF	η (%)	τ_{eff}/ms	L_n/μm	ω_{max}/Hz	R_D/Ω
0.01	13.06	0.71	0.69	6.46	201.94	43.7	3.12	10.7
0.03	13.03	0.71	0.73	6.75	175.83	44.6	3.77	4.86
0.05	12.39	0.70	0.75	6.44	147.46	44.7	3.06	3.08

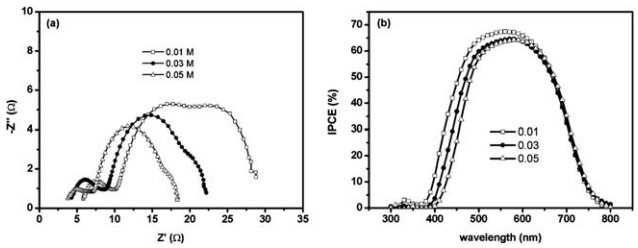

Fig. 5 (a) Nyquist plots of DSSCs containing different concentration of I_2 determined under an AM 1.5G solar illumination of 100 mW cm^{-2}. The thickness of the TiO_2 photoelectrode is 28 μm. (b) IPCE spectra of DSSC with different concentration of I_2.

similar. The electron transport resistance (R_w) (approximately 4 Ω) fluctuated with an increase in concentration of I_2. The concentration of I_2 also did not significantly affect the recombination resistance R_k at the photoelectrode. The effective electron diffusion length L_n was considered to evaluate the charge collection efficiency. A larger L_n contributes to a larger J_{SC}.[24] The L_n can be calculated according to the equation: $L_n = L(R_w/R_k)^{1/2}$. Table 3 shows that the observed L_n did not significantly change with various concentration of I_2 (less than 0.05 M). Fig. 5 (b) shows the incident photon to current efficiency (IPCE). The IPCE curves reveal a downward shift in the wavelength range from 400 to 600 nm with increasing concentration of I_2. The decrease in IPCE is due to I^-/I_3^- absorbing incident light in the back-illuminated device. As a consequence, reducing the concentration of I_2 enhances the light harvesting efficiency and contributed to improving J_{SC}, and the other contributing factors can be excluded.

4. Conclusions

In summary, this study reports the preparation of sponge-like TiO_2 formed on Ti substrates by H_2O_2 as an underlayer for DSSC. Compared with surface polished/$TiCl_4$ treatment on Ti substrates, the open current voltage, fill factor, and the efficiency of the DSSC using the H_2O_2 treated Ti substrate were improved by an increase in the contact area and favor adhesion at the Ti/TiO_2 interface. The significantly reduced charge transfer resistance at the Ti/TiO_2 interface made a very large contribution to the improvement of the FF. The increased electron density and the prolonged electron life time explained the improvement of V_{OC}. The resistance of I_3^- diffusion increased with decreasing concentration of I_3^- leading to a lower FF. The similar effective electron diffusion length and the upward shift of IPCE with a decreasing concentration of I_3^- indicate the improvement of light harvesting to increase J_{SC}. Surface modification by H_2O_2 oxidation combined with the optimized thickness of TiO_2 and concentration of I_2 achieved a high energy conversion efficiency of 6.75% for the back-illuminated DSSCs.

Acknowledgements

The financial support provided by Bureau of Energy (Grant No. 9455DI2110) is gratefully acknowledged.

References

1 M. K. Nazeeruddin, F. De Angelis, S. Fantacci, A. Selloni, G. Viscardi, P. Liska, S. Ito, B. Takeru and M. G. Grätzel, *J. Am. Chem. Soc.*, 2005, **48**, 16835.
2 C. Y. Jiang, X. W. Sun, K. W. Tan, G. Q. Lo, A. K. K. Kyaw and D. L. Kwong, *Appl. Phys. Lett.*, 2008, **92**, 143101.
3 S. Ito, N. L. C. Ha, G. Rothenberger, P. Liska, P. Comte, S. M. Zakeeruddin, P. Pechy, M. K. Nazeeruddin and M. Gratzel, *Chem. Commun.*, 2006, **38**, 4004.
4 Y. Saito, S. Uchida, T. Kubo and H. Segawa, *Thin Solid Films*, 2010, **518**, 3033.
5 H. G. Yun, Y. Jun, J. Kim, B. S. Bae and M. G. Kang, *Appl. Phys. Lett.*, 2008, **93**, 13311.
6 K. Onoda, S. Ngamsinlapasathian, T. Fujieda and S. Yoshikawa, *Sol. Energy Mater. Sol. Cells*, 2007, **91**, 1176.
7 K. Miettunen, J. Halme, M. Toivola and P. Lund, *J. Phys. Chem. C*, 2008, **112**, 4011.
8 S. Ito, P. Liska, P. Comte, R. L. Charvet, P. Pechy, U. Bach, L. Schmidt-Mende, S. M. Zakeeruddin, A. Kay, M. K. Nazeeruddin and M. Grätzel, *Chem. Commun.*, 2005, **34**, 4351.
9 T. W. Hamann, O. K. Farha and J. T. Hupp, *J. Phys. Chem. C*, 2008, **112**, 19756.
10 T. S. Kang, S. H. Moon and K. J. Kim, *J. Electrochem. Soc.*, 2002, **149**, E155.
11 B. Yoo, K. Kim, D. K. Lee, M. J. Ko, H. Lee, Y. H. Kim, W. M. Kim and N. G. Park, *J. Mater. Chem.*, 2010, **20**, 4392.
12 B. Yoo, K. J. Kim, S. Y. Bang, M. J. Ko, K. Kim and N. G. Park, *J. Electroanal. Chem.*, 2010, **638**, 161.
13 P. J. Cameron and L. M. Peter, *J. Phys. Chem. B*, 2005, **109**, 7392.
14 J. H. Park, Y. Jun, H. G. Yun, S. Y. Lee and M. G. Kang, *J. Electrochem. Soc.*, 2008, **155**, F145.
15 W. W. Tan, X. Yin, X. M. Zhou, J. B. Zhang, X. R. Xiao and Y. Lin, *Electrochim. Acta*, 2009, **54**, 4467.
16 S. Ito, T. N. Murakami, P. Comte, P. Liska, C. Gratzel, M. K. Nazeeruddin and M. Grätzel, *Thin Solid Films*, 2008, 4613.
17 J. Bisquert, *J. Phys. Chem. B*, 2002, **106**, 325.
18 M. Adachi, M. Sakamoto, J. T. Jiu, Y. Ogata and S. Isoda, *J. Phys. Chem. B*, 2006, **110**, 13872.
19 K. P. Wang and H. S. Teng, *Phys. Chem. Chem. Phys.*, 2009, **11**, 9489.
20 J. Xia, N. Masaki, K. Jiang and S. Yanagida, *J. Phys. Chem. B*, 2006, **110**, 25222.
21 Q. Wang, Z. Zhang, S. M. Zakeeruddin and M. Gratzel, *J. Phys. Chem. C*, 2008, **112**, 7084.
22 Z. S. Wang, H. Kawauchi, T. Kashima and H. Arakawa, *Coord. Chem. Rev.*, 2004, **248**, 1381.
23 T. Hoshikawa, T. Ikebe, R. Kikuchi and K. Eguchi, *Electrochim. Acta*, 2006, **51**, 5286.
24 Q. Wang, S. Ito, M. Gratzel, F. Fabregat-Santiago, I. Mora-Sero, J. Bisquert, T. Bessho and H. Imai, *J. Phys. Chem. B*, 2006, **110**, 25210.